

# Spontaneously quenched gamma-ray spectra from compact sources

M. Petropoulou, D. Arfani and A. Mastichiadis

Department of Physics, University of Athens, Panepistimiopolis, GR 15783 Zografos, Greece

Received.../Accepted...

## ABSTRACT

**Aims.** We study a mechanism for producing intrinsic broken power-law  $\gamma$ -ray spectra in compact sources. This is based on the principles of automatic photon quenching, according to which,  $\gamma$ -rays are being absorbed on spontaneously produced soft photons, whenever the injected luminosity in  $\gamma$ -rays lies above a certain critical value.

**Methods.** We derive an analytical expression for the critical  $\gamma$ -ray compactness in the case of power-law injection. For the case where automatic photon quenching is relevant, we calculate analytically the emergent steady-state  $\gamma$ -ray spectra. We perform also numerical calculations in order to back up our analytical results.

**Results.** We show that a spontaneously quenched power-law  $\gamma$ -ray spectrum obtains a photon index  $3\Gamma/2$ , where  $\Gamma$  is the photon index of the power-law at injection. Thus, large spectral breaks of the  $\gamma$ -ray photon spectrum, e.g.  $\Delta\Gamma \gtrsim 1$ , can be obtained by this mechanism. We also discuss additional features of this mechanism that can be tested observationally. Finally, we fit the multiwavelength spectrum of a newly discovered blazar (PKS 0447-439) by using such parameters, as to explain the break in the  $\gamma$ -ray spectrum by means of spontaneous photon quenching, under the assumption that its redshift lies in the range  $0.1 < z < 0.24$ .

**Key words.** radiation mechanisms: non-thermal – gamma-rays: general – BL Lacertae objects: general

## 1. Introduction

The production and radiation transfer of high-energy  $\gamma$ -rays is a physical problem that has attained a lot of attention over the last forty years since it can be applied on compact high-energy emitting astrophysical sources, such as Active Galactic Nuclei (AGN) and Gamma-Ray Bursts. Photon-photon absorption, in particular, turns out to be a significant physical process in compact X-ray and  $\gamma$ -ray emitting sources that results in electromagnetic (EM) cascades (e.g. Jelley (1966); Herterich (1974)). The effects of EM cascades can be studied within either a linear or non-linear framework. In the first approach (e.g. Protheroe (1986)), the number density of target photons is assumed to be fixed, whereas in the second one, the produced electron/positron pairs produce photons, which on their turn serve as targets for photon-photon absorption (Kazanas 1984; Zdziarski & Lightman 1985; Svensson 1987). The first analytical studies of EM cascades were then followed by numerical works, which aimed at computing time-dependent solutions to the kinetic equations of electrons and photons taking photon-photon annihilation into account (Coppi 1992; Mastichiadis & Kirk 1995; Stern et al. 1995; Böttcher & Chiang 2002). These algorithms are now commonly used in source modelling (Mastichiadis & Kirk 1997; Kataoka et al. 2000; Konopelko et al. 2003; Katarzyński et al. 2005).

However, intrinsically non-linear effects in EM cascades initiated by photon-photon absorption have only recently gained attention. First, Stawarz & Kirk (2007) – from this point on SK07 – studied the case where no soft (target) photons are present in a source. They investigated the nec-

essary conditions under which  $\gamma$ -ray photons can cause runaway pair production and found that these conditions can be summarized only in a single quantity, the ‘critical’  $\gamma$ -ray compactness. This can be considered as an upper limit of the  $\gamma$ -ray compactness, that depends on parameters such as the magnetic field strength and the size of the source. If the injection compactness of very high energy (VHE) photons ( $\gtrsim 0.1$  TeV) is larger than the critical one, the following non-linear loop is self-sustained:  $\gamma$ -ray photons are absorbed on soft photons emitted by the produced pairs through synchrotron radiation.

The work of SK07 was then expanded by Petropoulou & Mastichiadis (2011) – henceforth PM11 – mainly by taking into account continuous energy losses of the produced pairs. The non-linear loop of processes called ‘automatic photon quenching’ by SK07 can be the core of other more complex ones. In particular, Petropoulou & Mastichiadis (2012b) or just PM12b from this point on, have attributed the production of VHE  $\gamma$ -rays to synchrotron emission from secondaries produced in charged pion decay, while pions were the result of photohadronic interactions between relativistic protons and soft photons. PM12b have shown that the system of protons and photons resembles that of a prey-predator one, whenever automatic photon quenching operates, and it shows interesting variability patterns, such as limit cycles<sup>1</sup>.

In the present work we continue the exploration of spontaneous photon quenching by studying the case of power-

<sup>1</sup> Similar results are presented in Mastichiadis et al. (2005) but they are caused by a different intrinsic non-linear process known as the ‘PPS-loop’ (Kirk & Mastichiadis 1992).

low  $\gamma$ -ray injection in the source and, in that sense, it can be considered as a continuation of the aforementioned works. There were two main motivations of our present study: (i)  $\gamma$ -ray spectra emitted by a power-law distribution of relativistic particles through some radiation mechanism, e.g. synchrotron radiation and inverse Compton scattering, can be modelled by a power-law, at least partially and (ii) if spontaneous photon absorption affects part of the  $\gamma$ -ray injection spectrum, spectral breaks are produced; we believe that this requires further investigation, as it is an *intrinsic* mechanism for producing breaks in a  $\gamma$ -ray spectrum and it could be of relevance to recent results regarding  $\gamma$ -ray emitting blazars.

The present paper is structured as follows: in section 2 we derive an analytical expression for the critical  $\gamma$ -ray compactness in the case of power-law injection using certain simplifying assumptions, while we comment also on the validity range of our result. In the case where spontaneous photon quenching becomes relevant, we show that a break at the steady-state  $\gamma$ -ray spectrum appears and we further calculate analytically the expected spectral change. In section 3 we derive numerically the critical compactness for a wide range of parameter values and examine the effects that a primary soft photon component in the source would have on  $\gamma$ -ray absorption. Possible implications of spontaneous absorption on  $\gamma$ -ray emitting blazars are presented in section 4. We also present a list of observationally tested characteristics that a spontaneously quenched source would, in principle, show. In the same section we further show that the spectral energy distribution (SED) of the newly discovered blazar PKS 0477-439 can be explained within the framework of automatic quenching. For the required transformations between the reference systems of the blazar and the observer we have adopted a cosmology with  $\Omega_m = 0.3$ ,  $\Omega_\Lambda = 0.7$  and  $H_0 = 70 \text{ km s}^{-1} \text{ Mpc}^{-1}$ .

## 2. Analytical approach

We consider a spherical region of radius  $R$  containing a magnetic field of strength  $B$ . We assume that  $\gamma$ -rays are being produced in this volume by some non-thermal emission process, e.g. proton synchrotron radiation. In our analysis however, the  $\gamma$ -ray production mechanism remains unspecified, since its exact nature does not play a role in the derivation of our results. Furthermore,  $\gamma$ -rays are being injected with a luminosity  $L_\gamma^{\text{inj}}$  that is related to the injected  $\gamma$ -ray compactness as

$$\ell_{\text{inj}} = \frac{L_\gamma^{\text{inj}} \sigma_T}{4\pi R m_e c^3}, \quad (1)$$

where  $\sigma_T$  is the Thomson cross section. Without any substantial soft photon population inside the source, the  $\gamma$ -rays will escape without any attenuation in one crossing time. However, as SK07 and PM11 showed, the injected  $\gamma$ -ray compactness cannot become arbitrarily high because, if a critical value is reached, the following loop starts operating: (i) Gamma-rays pair-produce on soft photons, which can be initially arbitrarily low inside the source; (ii) the produced electron-positron pairs are highly relativistic, since they are created with approximately half the energy of the initial  $\gamma$ -ray photon, and cool mainly by synchrotron radiation, thus acting as a source of soft photons; (iii) the emitted synchrotron photons have lower energy when compared to the  $\gamma$ -ray photons and serve as targets for more  $\gamma\gamma$  interactions.

There are two conditions that should be satisfied simultaneously for this network to occur:

### 1. *Feedback* criterion

This is related to the energy threshold condition for photon-photon absorption and it requires that the synchrotron photons emitted from the pairs have sufficient energy to pair-produce on the  $\gamma$ -rays.

### 2. *Marginal stability* criterion

This is related to the optical depth for photon-photon absorption, which must be above unity in order to establish the growth of the instability.

By making suitable simplifying assumptions, one can derive an analytic relation for the first condition – see also SK07. Thus, combining (i) the threshold condition for  $\gamma\gamma$  absorption  $\epsilon x = 2$ , where  $\epsilon$  and  $x$  are the  $\gamma$ -ray and soft photon energies in units of  $m_e c^2$  respectively – this normalization will be used for all photon energies throughout the text unless stated otherwise – (ii) the fact that there is equipartition of energy among the created electron-positron pairs  $\gamma_e = \gamma = \epsilon/2$  and (iii) the assumption that the required soft photons are the synchrotron photons that the electrons/positrons radiate, i.e.,  $x_s = b\gamma^2$  where  $b = B/B_{\text{crit}}$  and  $B_{\text{crit}} = (m_e^2 c^3)/(e\hbar) \simeq 4.4 \times 10^{13} \text{ G}$ , one finds the following relation

$$\epsilon_q = \frac{2}{b^{1/3}} \quad (2)$$

that defines, for a certain magnetic field strength, the  $\gamma$ -ray photon energy above which automatic photon quenching becomes relevant.

In what follows, we will concentrate on the second condition, since our aim is to determine the value of the injected  $\gamma$ -ray compactness that ensures the growth of the instability. The corresponding calculations in the case of monoenergetic  $\gamma$ -ray injection can be found in SK07 and PM11. Here we focus on the more astrophysically relevant case of a power-law  $\gamma$ -ray injection. In order to treat this problem analytically we ‘discretize’ the power-law of  $\gamma$ -rays. In particular, we begin by calculating the critical compactness in the case where two monoenergetic  $\gamma$ -rays are injected. We repeat the calculation for the injection of three monoenergetic  $\gamma$ -rays and, finally, we generalize our result for  $N$  monoenergetic injection functions. Furthermore, our treatment is built upon the following assumptions & approximations:

1. Only two physical processes are taken into account, i.e. photon-photon absorption and synchrotron radiation of the produced pairs. Inverse Compton scattering of pairs on the synchrotron produced photons can be safely neglected because of the strong magnetic field, that is typically required for the automatic photon quenching loop to function, and the large<sup>2</sup> Lorentz factors of the produced pairs.
2. Only the equations describing the evolution of  $\gamma$ -rays and synchrotron (soft) photons are taken into account. The equation for the pairs is neglected, since these have synchrotron cooling timescales much smaller than the crossing time of the source. Thus, all the injected energy into pairs is transformed into synchrotron radiation.

<sup>2</sup> For a 100 GeV  $\gamma$ -ray photon, the dimensionless photon energy is  $\epsilon = 2 \times 10^5$  and the produced pairs have  $\gamma \approx \epsilon/2 = 10^5$ .

3. Synchrotron emissivity is approximated by a  $\delta$ -function, i.e.,  $j_s(x) = j_0\delta(x - x_s)$ , where  $x_s = b\gamma^2$  is the synchrotron critical energy.
4. The synchrotron energy losses of pairs are treated as ‘catastrophic’ escape from the considered energy range. In other words, an electron with Lorentz factor  $\gamma$  loses its energy by radiating synchrotron photons at energy  $b\epsilon^2/4$ .
5. The cross section of photon-photon absorption (in units of  $\sigma_T$ ) is approximated as

$$\sigma_{\gamma\gamma} \approx \sigma_0 \frac{H(x\epsilon - 2)}{x\epsilon}, \quad \sigma_0 = 0.652 \quad (3)$$

which is the same as the one given by Coppi & Blandford (1990) apart from the logarithmic term  $\ln(x)$ .

### 2.1. Marginal stability criterion for injection of two monoenergetic $\gamma$ -rays

Let us assume that  $\gamma$ -rays are being injected into the source at energies  $\epsilon_1$  and  $\epsilon_2$  ( $\epsilon_1 < \epsilon_2$ ) with compactnesses  $\ell_{\text{inj}}^{(i)}$  where  $i = 1, 2$ . We use such parameters in order to ensure that the  $\gamma$ -ray photon with the minimum energy satisfies the feedback criterion, i.e.  $\epsilon_1 > \epsilon_q = 2/b^{1/3}$ . Then, all higher energy  $\gamma$ -ray photons also satisfy the feedback criterion and the corresponding emitted synchrotron photons have energies  $x_{s,i} = b\epsilon_i^2/4$ . Gamma-ray photons with energy  $\epsilon_i$  can, therefore, be absorbed on both soft photon distributions because the energy threshold criterion is satisfied for all the four possible photon-photon interactions, i.e.  $\epsilon_i x_{s,j} > 2$  for  $i, j = 1, 2$ . We note also that we do not consider absorption of  $\gamma$ -rays on less energetic  $\gamma$ -rays. Moreover, the number densities of  $\gamma$ -ray photons and of the corresponding soft photons are denoted as  $n_\gamma^{(i)}$  and  $n_s^{(i)}$  respectively, where the symbols imply the relations  $n_\gamma^{(i)} \equiv n_\gamma(\epsilon)\delta(\epsilon - \epsilon_i)$  and  $n_s^{(j)} \equiv n_s(x)\delta(x - x_{s,j})$ ; the densities refer to the number of photons contained in a volume element  $\sigma_T R$ . In other words, if  $\hat{n}$  expresses the number of photons per erg per  $\text{cm}^3$ , then  $n = \hat{n}(\sigma_T R)(m_e c^2)$ . The dimensionless photon number densities are also related to the compactnesses through the relation

$$\ell_{\text{inj}}^{(i)} = \frac{n_\gamma^{(i)} \epsilon_i^2}{3}, \quad i = 1, 2 \quad (4)$$

for discrete monoenergetic injection<sup>3</sup>. Using the notations introduced above along with the assumptions (1)-(5) the system can be described by four equations

$$\frac{dn_\gamma^{(i)}}{d\tau} + n_\gamma^{(i)} = Q_{\text{inj}}^{(i)} + L_{\gamma\gamma}^{(ij)}, \quad i, j = 1, 2 \quad (5)$$

$$\frac{dn_s^{(i)}}{d\tau} + n_s^{(i)} = Q_{\gamma\gamma}^{(ij)}, \quad i, j = 1, 2 \quad (6)$$

where time is normalized with respect to the photon crossing/escape time from the source, i.e.  $\tau = ct/R$  and the operators  $L$  and  $Q$  denote losses and injection respectively;

<sup>3</sup> For a continuous power-law injection of photons the relation between the differential photon number density and compactness is  $\ell_{\text{inj}}(\epsilon) = n_\gamma(\epsilon)\epsilon/3$ , while the total injection compactness is calculated by  $\ell_{\text{inj}} = \int d\epsilon \ell_{\text{inj}}(\epsilon)$

the loss term in eq. (6) due to photon-photon absorption is omitted since it is negligible. We note that number densities and rates are equivalent in the dimensionless form of the above equations. The explicit expressions of the operators in eqs. (5) and (6) are

$$\begin{aligned} L_{\gamma\gamma}^{(ij)} &= -n_\gamma^{(i)} \int dx \sigma_{\gamma\gamma}(x\epsilon_i) n_s(x) \delta(x - x_{s,j}) = \\ &= -\frac{\sigma_0}{\epsilon_i x_{s,j}} n_\gamma^{(i)} n_s^{(j)} \end{aligned} \quad (7)$$

$$Q_{\gamma\gamma}^{(ij)} = Q_{\gamma\gamma}^0 n_\gamma^{(i)} n_s^{(j)} \quad (8)$$

$$Q_{\text{inj}}^{(i)} = \frac{3\ell_{\text{inj}}^{(i)}}{\epsilon_i^2}, \quad (9)$$

where the normalization constant  $Q_{\gamma\gamma}^0$  is calculated by equating the total  $\gamma$ -ray energy loss rate with the total energy injection rate into soft photons, i.e.  $-\int d\epsilon \epsilon L_{\gamma\gamma} = \int dx x Q_{\gamma\gamma}$ , and it is given by

$$Q_{\gamma\gamma}^0 = \frac{\sigma_0}{x_{s,j}^2}. \quad (10)$$

We note also that in the case of continuous power-law injection eq. (9) should be replaced by  $Q_{\text{inj}}(\epsilon) = 3\ell_{\text{inj}}(\epsilon)/\epsilon$ . The trivial stationary solution of eqs. (5) and (6) is  $(\bar{n}_\gamma^{(1)}, \bar{n}_\gamma^{(2)}, 0, 0)$ , where  $\bar{n}_\gamma^{(i)} = Q_{\text{inj}}^{(i)}$  and it corresponds to the case where the injection rate of  $\gamma$ -rays equals the photon escape rate from the source. Following the methodology described in SK07 and PM11 we introduce perturbations to all photon number densities and linearize the set of equations (5)-(6) around the trivial solution. The linearized system can be written in the form  $dY/d\tau = \mathbf{A}Y$  where

$$Y = \begin{pmatrix} n_\gamma^{\prime(1)} \\ n_\gamma^{\prime(2)} \\ n_s^{\prime(1)} \\ n_s^{\prime(2)} \end{pmatrix} \quad (11)$$

is the vector of the perturbed number densities and  $\mathbf{A}$  is the matrix of the linearized system of equations

$$\mathbf{A} = \begin{pmatrix} -1 & 0 & -\frac{\sigma_0}{\epsilon_1 x_{s,1}} \bar{n}_\gamma^{(1)} & -\frac{\sigma_0}{\epsilon_1 x_{s,2}} \bar{n}_\gamma^{(1)} \\ 0 & -1 & -\frac{\sigma_0}{\epsilon_2 x_{s,1}} \bar{n}_\gamma^{(2)} & -\frac{\sigma_0}{\epsilon_2 x_{s,2}} \bar{n}_\gamma^{(2)} \\ 0 & 0 & -1 + \frac{\sigma_0}{x_{s,1}^2} \bar{n}_\gamma^{(1)} & \frac{\sigma_0}{x_{s,2}^2} \bar{n}_\gamma^{(1)} \\ 0 & 0 & \frac{\sigma_0}{x_{s,1}^2} \bar{n}_\gamma^{(2)} & -1 + \frac{\sigma_0}{x_{s,2}^2} \bar{n}_\gamma^{(2)} \end{pmatrix}. \quad (12)$$

In order to build a finite number of soft photons in the source, the perturbations must grow with time. This is ensured, if, at least one of the eigenvalues of matrix  $\mathbf{A}$  is positive. After some algebraic manipulation we find that, indeed, one eigenvalue can become positive if the following condition holds

$$\frac{Q_{\text{inj}}^{(1)}}{\epsilon_1^4} + \frac{Q_{\text{inj}}^{(2)}}{\epsilon_2^4} \geq \frac{b^2}{16\sigma_0}. \quad (13)$$

The same methodology can be applied in the case where  $\gamma$ -rays are being injected as a  $\delta$ -function at three energies  $\epsilon_1 < \epsilon_2 < \epsilon_3$ . This leads to an analogous critical condition

$$\frac{Q_{\text{inj}}^{(1)}}{\epsilon_1^4} + \frac{Q_{\text{inj}}^{(2)}}{\epsilon_2^4} + \frac{Q_{\text{inj}}^{(3)}}{\epsilon_3^4} \geq \frac{b^2}{16\sigma_0}. \quad (14)$$

## 2.2. Critical compactness for power-law $\gamma$ -ray injection

The above can be generalized for the case of  $N$  monoenergetic  $\gamma$ -rays with energies  $\epsilon_1 < \epsilon_i < \epsilon_N$  in order to find the following marginal stability criterion

$$\sum_{i=1}^N \frac{Q_{\text{inj}}^{(i)}}{\epsilon_i^4} \geq \frac{b^2}{16\sigma_0}. \quad (15)$$

We have verified that the above relation applies also to cases where the feedback criterion is not satisfied for  $\gamma$ -rays of the minimum energy but for higher energy photons, i.e.  $\epsilon_k = 2/b^{1/3}$  with  $k > 1$ , with only a slight modification: the summation starts from  $i = k$ . Moreover, if we assume that the injection rate of  $\gamma$ -ray photons can be modelled as a power-law, e.g.

$$Q_{\text{inj}}^{(i)} = Q_0 \left( \frac{\epsilon_i}{\epsilon_1} \right)^{-\Gamma}, \quad i = 1, \dots, N \quad (16)$$

the criterion of eq. (15) takes the form

$$Q_0 \sum_{i=1}^N \epsilon_i^{-\Gamma-4} \geq \frac{b^2}{16\sigma_0 \epsilon_1^\Gamma}. \quad (17)$$

If  $N \rightarrow \infty$  and  $(\epsilon_{i+1} - \epsilon_i) \rightarrow 0$ , the discrete sum of eq. (17) can be transformed into an integral which leads to

$$Q_0 \geq \frac{b^2 \epsilon_1^{-\Gamma}}{16\sigma_0} \frac{\Gamma + 3}{\epsilon_1^{-\Gamma-3} - \epsilon_N^{-\Gamma-3}}. \quad (18)$$

Finally, if we replace the normalization constant  $Q_0$  by the integrated  $\gamma$ -ray compactness over all photon energies (see also comment on eq. (9)) using

$$\ell_{\text{inj}} = \frac{1}{3} \int_{\epsilon_1}^{\epsilon_N} d\epsilon Q_0 \epsilon \left( \frac{\epsilon}{\epsilon_1} \right)^{-\Gamma} \quad (19)$$

we find that  $\ell_{\text{inj}} \geq \ell_{\gamma, \text{cr}}$  where  $\ell_{\gamma, \text{cr}}$  is the critical compactness for a power-law  $\gamma$ -ray injection. This has a rather compact form

$$\ell_{\gamma, \text{cr}} = \frac{b^2}{48\sigma_0} \begin{cases} \frac{(\Gamma+3)(\epsilon_{\text{min}}^{-\Gamma+2} - \epsilon_{\text{max}}^{-\Gamma+2})}{(\Gamma-2)(\epsilon_{\text{M}}^{-\Gamma-3} - \epsilon_{\text{max}}^{-\Gamma-3})}, & \text{for } \Gamma \neq 2 \\ \frac{(\Gamma+3)}{(\epsilon_{\text{M}}^{-\Gamma-3} - \epsilon_{\text{max}}^{-\Gamma-3})} \ln \left( \frac{\epsilon_{\text{max}}}{\epsilon_{\text{min}}} \right), & \text{for } \Gamma = 2, \end{cases} \quad (20)$$

where  $\epsilon_{\text{min}} \equiv \epsilon_1$ ,  $\epsilon_{\text{max}} \equiv \epsilon_N$  and  $\epsilon_{\text{M}} = \max[\epsilon_{\text{min}}, \epsilon_{\text{q}}]$  – for the definition of  $\epsilon_{\text{q}}$  see eq. (2).

We were able to derive an analytical and rather simple expression of the critical compactness in the case of power-law injection at the cost, however, of a series of approximations/assumptions that may limit the validity range of our result. It is reasonable therefore, before closing the present section to check the range of validity of eq. (20). For this, we made a comparison between this expression and the numerically derived values<sup>4</sup>, which is exemplified in Fig. 1. Both panels show the dependence of  $\ell_{\gamma, \text{cr}}$  on  $\epsilon_{\text{min}}$  for two different pairs of photon indices marked on the plots. Lines and symbols are used for plotting the analytically and numerically derived values respectively, while different types of lines/symbols correspond to different values of the photon index. For values of  $\epsilon_{\text{min}}$  below  $\epsilon_{\text{q}}$ , which for the values

<sup>4</sup> For more details on the numerical code used, see section 3.

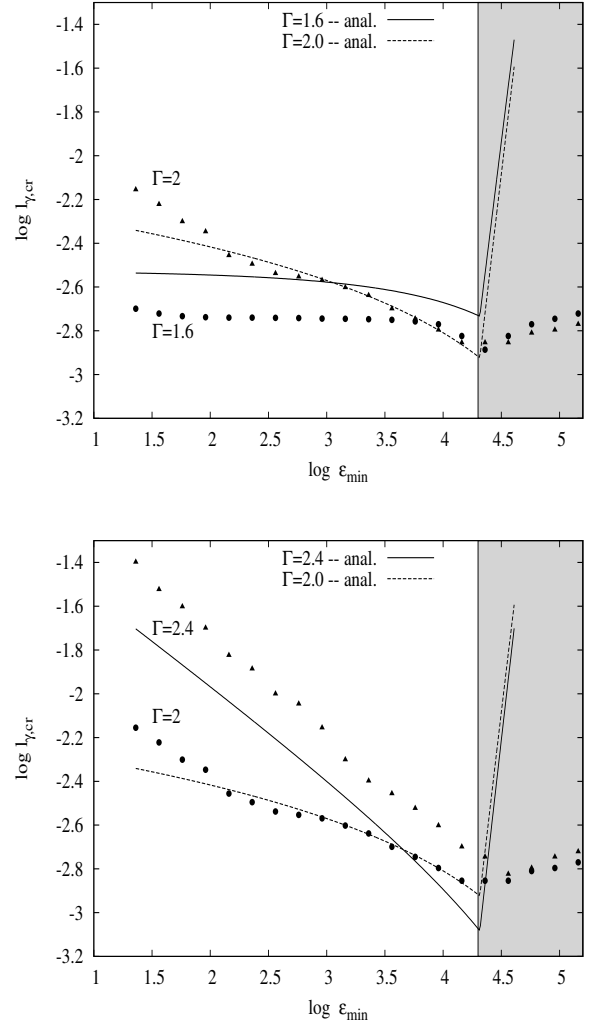


**Fig. 1.** Top panel: critical compactness  $\ell_{\gamma, \text{cr}}$  as a function of the minimum energy of the  $\gamma$ -ray spectrum  $\epsilon_{\text{min}}$  for  $\Gamma = 1.6$  (solid line) and  $\Gamma = 2$  (dashed line). The numerically derived values for the two cases are shown with circles and triangles respectively. Bottom panel: same as in top panel except for different photon indices, which are marked on the plot. Other parameters used are:  $\epsilon_{\text{max}} = 2.3 \times 10^5$  (in  $m_e c^2$  units),  $B = 40$  G and  $R = 3 \times 10^{16}$  cm. In both panels the grey area denotes the region where  $\epsilon_{\text{min}} > \epsilon_{\text{q}}$  – for the definition of  $\epsilon_{\text{q}}$  see text.

used in this example equals  $2 \times 10^4$ , we find a good agreement between our analytical and numerical results, apart from some numerical factor of  $\simeq 2$ ; notice that the dependence of  $\ell_{\gamma, \text{cr}}$  given by eq. (20) on  $\epsilon_{\text{min}}$  coincides with the one determined numerically. However, the analytical solution of  $\ell_{\gamma, \text{cr}}$  fails in the energy range of  $\epsilon_{\text{min}} \geq \epsilon_{\text{q}}$ , since, in this regime, approximation (4) listed at the beginning of section 2 proves to be crude.

## 2.3. Steady state $\gamma$ -ray quenched spectrum

Assuming that the injected  $\gamma$ -ray compactness exceeds the critical value derived in the previous section, we search for steady-state solutions of the system. There is a main difference between the analytical approach that we follow in this section and the one presented in section 2.1: here we

take into account the cooling of pairs due to synchrotron radiation, i.e. synchrotron losses are treated as a continuous energy loss mechanism. For this reason, in addition to the equations of  $\gamma$ -rays and soft photons, we include in our analysis a third equation for electron/positron pairs or simply electrons from this point on. Dropping the time derivatives, the kinetic equations for  $\gamma$ -rays, soft photons and electrons are written respectively as

$$n_\gamma(\epsilon) = Q_{\text{inj}}^\gamma(\epsilon) + L_{\gamma\gamma}^\gamma(\epsilon) \quad (21)$$

$$n_s(x) = Q_{\text{syn}}^s(x) \quad (22)$$

and

$$n_e(\gamma) = Q_{\gamma\gamma}^e(\gamma) + L_{\text{syn}}^e(\gamma), \quad (23)$$

where  $n_e$  is the dimensionless electron number density and an electron escape timescale  $t_{e,\text{esc}} = t_{\text{cr}}$  was assumed. All normalizations and approximations – apart from the fourth in our list – are the same as in section 2.1. The synchrotron emissivity is approximated by a  $\delta$ -function – see section 2.1. We note that in what follows we can safely neglect electron escape from the source, since, for magnetic field strengths relevant to automatic quenching, synchrotron cooling is the dominant term in the electron equation; thus, the left hand side of eq. (23) is essentially equal to zero. Then, the injection and loss operators take the following forms:

$$Q_{\text{inj}}^\gamma = Q_0 \epsilon^{-\Gamma} H(\epsilon - \epsilon_{\text{min}}) H(\epsilon_{\text{max}} - \epsilon) \quad (24)$$

$$Q_{\text{syn}}^s = \alpha_1 x^{-1/2} n_e \left( \sqrt{\frac{x}{b}} \right) \quad (25)$$

$$Q_{\gamma\gamma}^e = -4\mathcal{L}_{\gamma\gamma}^\gamma, \quad (26)$$

where the form of  $Q_{\text{syn}}^s$  implies the use of a  $\delta$ -function for the synchrotron emissivity (see e.g. Mastichiadis & Kirk (1995)) and  $\alpha_1 = (2/3)\ell_B b^{-3/2}$ . The loss operators are given by

$$\mathcal{L}_{\gamma\gamma}^\gamma = -n_\gamma(\epsilon) \int_0^{x_{\text{max}}} dx \sigma_{\gamma\gamma}(x\epsilon) n_s(x) \quad (27)$$

$$\mathcal{L}_{\text{syn}}^e = +\alpha_2 \frac{\partial}{\partial \gamma} (\gamma^2 n_e) \quad (28)$$

where  $x_{\text{max}} = b\gamma_{\text{max}}^2 = b\epsilon_{\text{max}}^2/4$  is the maximum energy of the produced soft photon distribution<sup>5</sup>,  $\alpha_2 = 4\ell_B/3$  with  $\ell_B = \sigma_T R U_B / m_e c^2$  being the ‘magnetic compactness’ and  $\sigma_{\gamma\gamma}$  is the dimensionless (in units of  $\sigma_T$ ) cross section for photon-photon absorption (see point (5) of section 2). Within this approximation eq. (27) takes the form

$$\mathcal{L}_{\gamma\gamma}^\gamma = -n_\gamma(\epsilon) \int_{2/\epsilon}^{x_{\text{max}}} dx \sigma_0 \frac{n_s(x)}{x\epsilon} \quad (29)$$

which further implies that  $\gamma$ -rays with energy  $\epsilon < \epsilon_{\text{br}} \equiv 2/x_{\text{max}}$  cannot be absorbed. Thus, pairs with  $\gamma < \gamma_{\text{br}} \equiv \epsilon_{\text{br}}/2$  cannot be produced, i.e. the injection term in eq. (23) vanishes. The above can be summarized by inserting the step function  $H(\epsilon - \epsilon_{\text{br}})$  in the expression of  $\mathcal{L}_{\gamma\gamma}^\gamma$  given by eq. (29). On the one hand, for  $\gamma < \gamma_{\text{br}}$  the electron distribution has the trivial form  $n_e \propto \gamma^{-2}$ . On the other hand,

for  $\gamma \geq \gamma_{\text{br}}$ , the distribution is determined by synchrotron losses and pair injection.

We now proceed to calculate the electron distribution for  $\gamma > \gamma_{\text{br}}$ . After having inserted the above expressions for the operators into eqs. (21)–(23), we combine them into one non-linear integrodifferential equation, where the unknown function is  $n_e(\gamma)$ :

$$-\alpha_2 \frac{d}{d\gamma} (\gamma^2 n_e) = 4Q_{\text{inj}}^\gamma(2\gamma) H(\gamma - \gamma_{\text{br}}) \frac{I(n_e; \gamma)}{1 + I(n_e; \gamma)}, \quad (30)$$

where

$$I(n_e; \gamma) = \frac{\alpha_1 \sigma_0}{2\gamma} \int_{1/\gamma}^{x_{\text{max}}} dx n_e \left( \sqrt{\frac{x}{b}} \right) x^{-3/2}. \quad (31)$$

Integration of eq. (30) leads to

$$\alpha_2 [\gamma'^2 n_e(\gamma')]_{\gamma_{\text{max}}}^\gamma = \frac{Q_0}{2^{\Gamma-2}} \int_{\gamma_{\text{min}}^{\text{eff}}}^{\gamma_{\text{max}}} d\gamma' \gamma'^{-\Gamma} \frac{I(n_e; \gamma')}{1 + I(n_e; \gamma')}, \quad (32)$$

where we have used the notation  $[Y]_{x_1}^{x_2} \equiv Y(x_2) - Y(x_1)$  and  $\gamma_{\text{min}}^{\text{eff}} = \max[\gamma, \gamma_{\text{min}}, \gamma_{\text{br}}]$ . If  $\gamma_{\text{br}} > \gamma_{\text{min}}$  then  $\gamma_{\text{min}}^{\text{eff}} = \gamma$ , whereas if  $\gamma_{\text{br}} < \gamma_{\text{min}}$  then  $\gamma_{\text{min}}^{\text{eff}}$  can be equal either to  $\gamma_{\text{min}}$  or  $\gamma$ . The condition  $\gamma_{\text{br}} < \gamma_{\text{min}}$  corresponds to the physical case where the entire  $\gamma$ -ray power-law spectrum is affected by automatic quenching. Therefore, the steady-state  $\gamma$ -ray spectrum will show, in general, no break (see also numerical example in Fig. 8 of PM11). Since in the present work we are interested in producing broken power-law  $\gamma$ -ray spectra, we will examine only the case where  $\gamma_{\text{br}} > \gamma_{\text{min}}$  and therefore  $\gamma_{\text{min}}^{\text{eff}} = \gamma$ . Since an exact solution of eq. (32) cannot be obtained analytically, we assume a certain form for the solution we are searching for. A reasonable ‘guess’ is that the electron distribution is a power-law, i.e.  $n_e = N_0 \gamma^{-p}$ , where  $N_0$  and  $p$  are the parameters to be defined. Inserting this function into eq. (32) we obtain

$$\alpha_2 N_0 [\gamma'^{-p+2}]_{\gamma_{\text{max}}}^\gamma = \frac{Q_0}{2^{\Gamma-2}} \int_\gamma^{\gamma_{\text{max}}} d\gamma' \frac{A(N_0, p) \gamma'^{-\Gamma+\beta}}{1 + A(N_0, p) \gamma'^\beta}, \quad (33)$$

where  $\beta = \frac{p-1}{2}$  and  $A(N_0, p) = N_0 b^{p/2} \alpha_1 \sigma_0 / (p+1)$  is a function only of the unknown parameters for fixed values of the magnetic field and source size. We note also that we have neglected the contribution of terms calculated at the upper limit ( $x_{\text{max}}$ ) while performing the integral  $I(\gamma')$ , so that the solution of the final integral appearing at the right hand side of eq. (33) can be expressed in closed form as

$$\left[ \frac{A \gamma'^{-\Gamma+\beta+1}}{-\Gamma+\beta+1} {}_2F_1 \left( 1, 1 + \frac{1-\Gamma}{\beta}, 2 + \frac{1-\Gamma}{\beta}; -A \gamma'^\beta \right) \right]_\gamma^{\gamma_{\text{max}}}, \quad (34)$$

where  ${}_2F_1(a, b, c; z)$  is the Gauss hypergeometric function. Without making any further approximations the above equation cannot be solved for  $p$  and  $N_0$  analytically. However, if the term  $A \gamma'^\beta$  inside the integral is much larger than unity, this is, then, greatly simplified and eq. (33) takes the form

$$-\alpha_2 N_0 [\gamma'^{-p+2}]_\gamma^{\gamma_{\text{max}}} \approx \frac{Q_0 2^{-\Gamma+2}}{-\Gamma+1} [\gamma'^{-\Gamma+1}]_\gamma^{\gamma_{\text{max}}}, \quad (35)$$

which is satisfied for

$$p = \Gamma + 1 \quad \text{and} \quad (36)$$

$$N_0 = \frac{2^{-\Gamma+2} Q_0}{\alpha_2 (\Gamma - 1)}. \quad (37)$$

<sup>5</sup> As a minimal condition, we assume that the energy threshold criterion for automatic photon quenching is satisfied at least from the maximum energy  $\gamma$ -rays, i.e.  $b\epsilon_{\text{max}}^3 > 8$ .

The above solution is valid as long as  $\Gamma \neq 1$ . In the opposite case, one should search for more general forms of the electron distribution, i.e.  $n_e(\gamma) \propto N_0(\gamma)\gamma^{-p}$  and follow the same procedure. However, for the purposes of the present work, the solution for  $\Gamma \neq 1$  is sufficient. Summarizing, the electron distribution is given by

$$n_e(\gamma) = N_0\gamma_{\text{br}}^{-\Gamma-1} \begin{cases} \left(\frac{\gamma}{\gamma_{\text{br}}}\right)^{-2}, & \text{for } \gamma_{\text{min}} \leq \gamma \leq \gamma_{\text{br}}, \\ \left(\frac{\gamma}{\gamma_{\text{br}}}\right)^{-\Gamma-1}, & \text{for } \gamma_{\text{br}} < \gamma \leq \gamma_{\text{max}} \end{cases} \quad (38)$$

where we have demanded the solution to be continuous at  $\gamma = \gamma_{\text{br}}$ . Notice that the slope of the electron distribution above  $\gamma_{\text{br}}$  is  $\Gamma + 1$ , i.e. steeper than that at injection (see term  $\gamma'^{-\Gamma}$  in eq. (32)) by one. This denotes the efficient synchrotron cooling of the whole distribution. We emphasize that the results for  $\gamma \gtrsim \gamma_{\text{br}}$  should be taken cautiously into consideration, since the above solution is not valid for all  $\gamma$  above  $\gamma_{\text{br}}$ ; we remind that it was derived under the approximation  $A\gamma^\beta > 1$  or equivalently

$$\gamma > \left( \frac{2^{\Gamma-1}(\Gamma+1)(\Gamma-1)\alpha_2}{Q_0\alpha_1\sigma_0 b^{\frac{\Gamma+1}{2}}} \right)^{2/\Gamma}. \quad (39)$$

After having determined the form of the electron distribution we can then calculate the steady-state solutions for  $\gamma$ -rays and soft photons. For  $\epsilon \leq \epsilon_{\text{br}}$  the injected spectrum remains unaffected by automatic quenching, whereas for  $\epsilon > \epsilon_{\text{br}}$ , the solution  $n_\gamma(\epsilon)$  can be found by inserting first the second branch of  $n_e$  into eq. (22) and then use the derived expression for  $n_s(x)$  into eq. (21). The results are summarized below

$$n_\gamma(\epsilon) = Q_0\epsilon^{-\Gamma}, \quad \epsilon_{\text{min}} \leq \epsilon \leq \epsilon_{\text{br}} \quad (40)$$

$$n_\gamma(\epsilon) = \frac{Q_0\epsilon^{-\Gamma}}{1 + \frac{F}{\epsilon} \left( \left(\frac{2}{\epsilon}\right)^{-\alpha} - x_{\text{max}}^{-\alpha} \right)}, \quad \epsilon_{\text{br}} < \epsilon \leq \epsilon_{\text{max}}$$

where  $\alpha = \Gamma/2 + 1$  and

$$F = \frac{8b^{\frac{\Gamma+1}{2}}Q_0\sigma_0\alpha_1}{2^\Gamma(\Gamma-1)(\Gamma+2)\alpha_2} \quad (41)$$

As the solution for  $n_e$  is not valid for  $\gamma \gtrsim \gamma_{\text{br}}$  (see eq. (39)), the behaviour of  $n_\gamma$  close to the transition, i.e. for  $\epsilon \gtrsim \epsilon_{\text{br}}$ , should also be considered with caution. The validity range set by eq. (39) can be translated into terms of photon energies, i.e.  $\epsilon > \epsilon_*$ , where

$$\epsilon_* = \left( \frac{2^{\frac{3\Gamma}{2}}(\Gamma-1)(\Gamma+2)\alpha_2}{4Q_0\sigma_0 b^{\frac{\Gamma+1}{2}}\alpha_1} \right)^{\frac{2}{\Gamma}} \quad (42)$$

It can be easily verified that, for  $\epsilon > \epsilon_*$  the second term in the denominator of  $n_\gamma$  is larger than unity<sup>6</sup>, which simplifies the functional dependence of  $n_\gamma$  on energy, i.e.  $n_\gamma \propto \epsilon^{-3\Gamma/2}$ . Summarizing, we find that the asymptotic photon index of a spontaneously quenched  $\gamma$ -ray spectrum is well defined and

<sup>6</sup> The physical interpretation of this condition is that the absorption term in the  $\gamma$ -ray photon equation is larger than the escape term. In this energy range, the photon distribution is determined mainly by the automatic quenching.

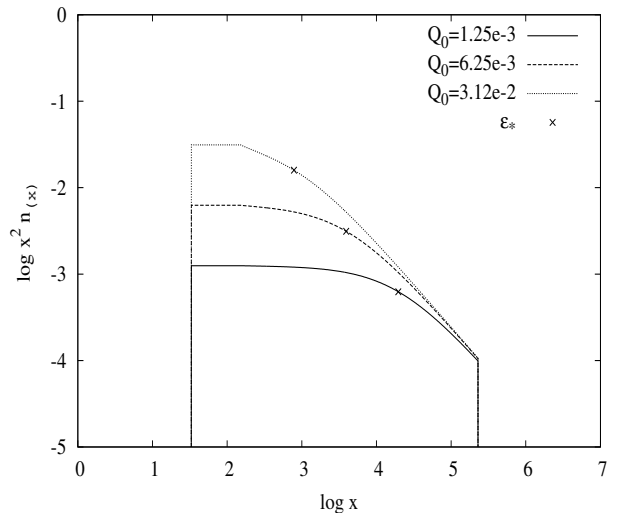


**Fig. 2.** Analytical solution of steady-state spontaneously quenched  $\gamma$ -ray spectra for different values of the injection parameter  $Q_0$  starting from  $1.25 \times 10^{-3}$ . Each value is increased by a factor of 5 over its previous one. X-symbols denote in each case the value of  $\epsilon_*$ . Other parameters used are:  $\Gamma = 2$ ,  $\epsilon_{\text{min}} = 33$ ,  $\epsilon_{\text{max}} = 2.3 \times 10^5$ ,  $B = 40$  G and  $R = 3 \times 10^{16}$  cm. The break energy is then  $\epsilon_{\text{br}} = 160$ .

it is given by  $3\Gamma/2$ ; this result is in complete agreement with the one derived numerically in PM11 – see Fig. 9 therein. The spectral break in the case of automatic quenching depends, therefore, linearly on the photon index at injection, i.e.  $\Delta\Gamma = \Gamma/2$ .

Figure 2 shows the  $\gamma$ -ray spectra given by eq. (40) for  $\Gamma = 2$  along with  $\epsilon_*$  (X-symbols) for different values of the injection parameter  $Q_0$  that ensure the operation of spontaneous photon quenching. Our solution for  $\epsilon > \epsilon_{\text{br}}$  becomes progressively valid over a larger range of energies as  $Q_0$  increases. Moreover, for the highest value of  $Q_0$ , the photon index of the quenched part of the spectrum is 3, i.e. it has obtained its asymptotic value defined by  $3\Gamma/2$ . The analytical solutions presented in Fig. 2 are compared to those derived using the numerical code described in the following section and PM11. Solid and dashed lines in Fig. 3 correspond to the analytical and numerical solutions respectively. The agreement between the two is better for larger values of the injection compactness, i.e. when the absorption term in the equation of  $\gamma$ -ray photons becomes larger.

Before closing the present section and for reasons of completeness we make a short comment on our choice of assuming continuous instead of catastrophic energy losses of electrons. We have also derived the steady-state solution in the case of monoenergetic injection of  $N$   $\gamma$ -rays using catastrophic losses. However, the obtained results, when compared to the numerically derived ones, were not reasonable, in the sense that no large spectral breaks were produced since  $\gamma$ -ray absorption was underestimated. The main reason behind this disagreement with the numerically derived results is the approximation (4). By assuming catastrophic losses of the produced pairs we neglect soft photons with  $x < be^2/4$ , i.e. we artificially decrease the optical depth for absorption of a  $\gamma$ -ray photon with certain energy  $\epsilon$ . Thus, although the assumption of catastrophic losses proves to be

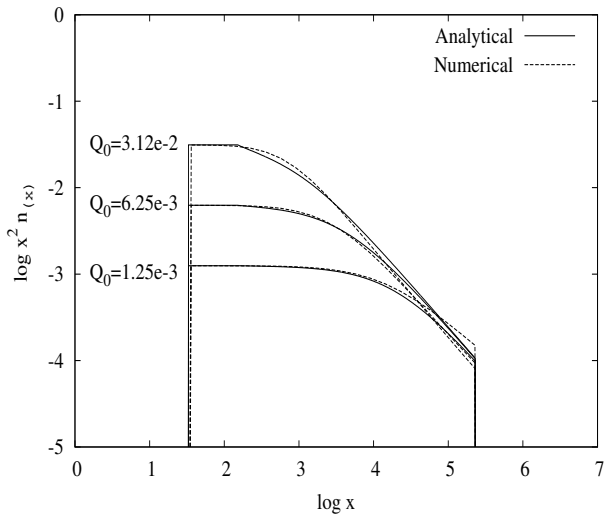


**Fig. 3.** Numerical (dashed lines) and analytical (solid lines) solutions for the steady-state  $\gamma$ -ray spectra. The injection rate increases from bottom to top starting from  $Q_0 = 1.25 \times 10^{-3}$ . The parameters used are the same as in Fig. 2.

sufficient for the derivation of  $\ell_{\gamma,cr}$  (section 2.1) it proves to be too crude for more quantitative results.

### 3. Numerical approach

In this section we will present

- (i) the dependence of the critical injection compactness on various parameters, e.g. on the minimum and maximum energy of injected  $\gamma$ -rays, as well as on the  $\gamma$ -ray photon index, for a wide range of values.
- (ii) the effects that the presence of low-energy photons has on the automatic absorption of  $\gamma$ -rays.

For a detailed study of the above a numerical treatment is required; as far as the first point is concerned, we have already shown that the analytical approach breaks down e.g. for sufficiently high values of the minimum energy of injected  $\gamma$ -rays – see section 2.1.

To numerically investigate the properties of quenching one needs to solve again the system of eqs. (5)-(6), where the discretized photon number densities should be replaced by their continuous functional form. For completeness we have augmented it to include more physical processes. As in the numerical code, there is no need to treat the time-evolution of soft photons and  $\gamma$ -rays through separate equations, the system can be written:

$$\frac{\partial n_e(\gamma, t)}{\partial t} + \frac{n_e}{t_{e,esc}} = Q_{\gamma\gamma}^e + \mathcal{L}_{syn}^e + \mathcal{L}_{ics}^e \quad (43)$$

and

$$\frac{\partial n_\gamma(x, t)}{\partial t} + \frac{n_\gamma}{t_{\gamma,esc}} = \mathcal{L}_{\gamma\gamma}^\gamma + Q_{syn}^\gamma + Q_{ics}^\gamma + \mathcal{L}_{ssa}^\gamma + Q_{inj}^\gamma, \quad (44)$$

where  $n_e$  and  $n_\gamma$  are the differential electron and photon number densities, respectively, normalized as in section 2. Here we considered the following processes: (i) Photon-photon pair production, which acts as a source term for

electrons ( $Q_{\gamma\gamma}^e$ ) and a sink term for photons ( $\mathcal{L}_{\gamma\gamma}^\gamma$ ); (ii) synchrotron radiation, which acts as a loss term for electrons ( $\mathcal{L}_{syn}^e$ ) and a source term for photons ( $Q_{syn}^\gamma$ ); (iii) synchrotron self-absorption, which acts as a loss term for photons ( $\mathcal{L}_{ssa}^\gamma$ ) and (iv) inverse Compton scattering, which acts as a loss term for electrons ( $\mathcal{L}_{ics}^e$ ) and a source term for photons ( $Q_{ics}^\gamma$ ). In addition to the above, we assume that  $\gamma$ -rays are injected into the source through the term ( $Q_{inj}^\gamma$ ). The functional forms of the various rates have been presented elsewhere – Mastichiadis & Kirk (1995, 1997) and Petropoulou & Mastichiadis (2009). The photons are assumed to escape the source in one crossing time, therefore  $t_{\gamma,esc} = R/c$ . The electron physical escape timescale from the source  $t_{e,esc}$  is another free parameter which, however, is not important in our case. Thus, we will fix it at value  $t_{e,esc} = t_{\gamma,esc} = R/c$ . The final settings are the initial conditions for the electron and photon number densities. Because we are investigating the spontaneous growth of pairs and their emitted synchrotron photons, we assume that at  $t = 0$  there are no electrons in the source, so we set  $n_e(\gamma, 0) = \eta \rightarrow 0$ . Moreover, during the injection of photons in a certain  $\gamma$ -ray energy range it is important to keep the background photons used in the numerical code at a level as low as possible in order to avoid artificial growth of the instability.

#### 3.1. Critical $\gamma$ -ray compactness for power-law injection

The procedure we follow for the numerical determination of the critical compactness is as follows: we start by injecting  $\gamma$ -rays at a rather low rate in a specific energy range ( $\epsilon_{min}, \epsilon_{max}$ ), e.g.  $\ell_{inj} \simeq 10^{-5}$ , and then we increase  $\ell_{inj}$  over its previous value by a factor of 0.2 in logarithm. The increase of  $\ell_{inj}$  is directly related to the increase of the normalization  $Q_0$  of the injection  $\gamma$ -ray spectrum; we remind that  $\ell_{inj} = (Q_0/3)(\epsilon_{min}^{-\Gamma+2} - \epsilon_{max}^{-\Gamma+2})/(\Gamma-2)$  for  $\Gamma \neq 2$ . For each value we allow the system to reach a steady state and then we examine the shape of the  $\gamma$ -ray spectrum. We define as  $\ell_{\gamma,cr}$  that value of  $\ell_{inj}$  that causes the first deviation from the spectral shape at injection; for this reason, we consider it as a rather strict limit.

Figure 4 shows  $\ell_{\gamma,cr}$  as a function of  $\epsilon_{min}$  (top panel) or  $\epsilon_{max}$  (bottom panel) for three different slopes of the injection spectrum marked on the plot. Other parameters used are:  $B = 40$  G and  $R = 3 \times 10^{16}$  cm. In the top panel, the maximum energy of the power-law spectrum is fixed at  $\epsilon_{max} = 2.3 \times 10^5$ , whereas in the bottom panel the minimum energy is taken to be constant and equal to  $\epsilon_{min} = 1.4 \times 10^5$ . For soft injection spectra, e.g.  $\Gamma = 2.4$ , we find that  $\ell_{\gamma,cr}$  strongly depends on  $\epsilon_{min}$ . The situation is exactly the opposite for hard  $\gamma$ -ray spectra – see solid line in bottom panel of the same figure. The critical compactness that we derive for  $\epsilon_{min} \approx \epsilon_{max} \approx 2.5 \times 10^5$  is  $\ell_{\gamma,cr} \approx 2 \times 10^{-3}$  – see bottom panel of Fig. 4 – and it corresponds to monoenergetic  $\gamma$ -ray injection. Thus, it should be compared to  $\ell_{\gamma,cr} \approx 5 \times 10^{-4}$ , which was derived analytically in PM11 for  $\delta$ -function injection at  $\epsilon = 2.5 \times 10^5$  – see Fig. 2 therein. The difference between the two results is not worrying, since the analytical values in PM11 were about a factor of four lower than the accurate values that were derived numerically.

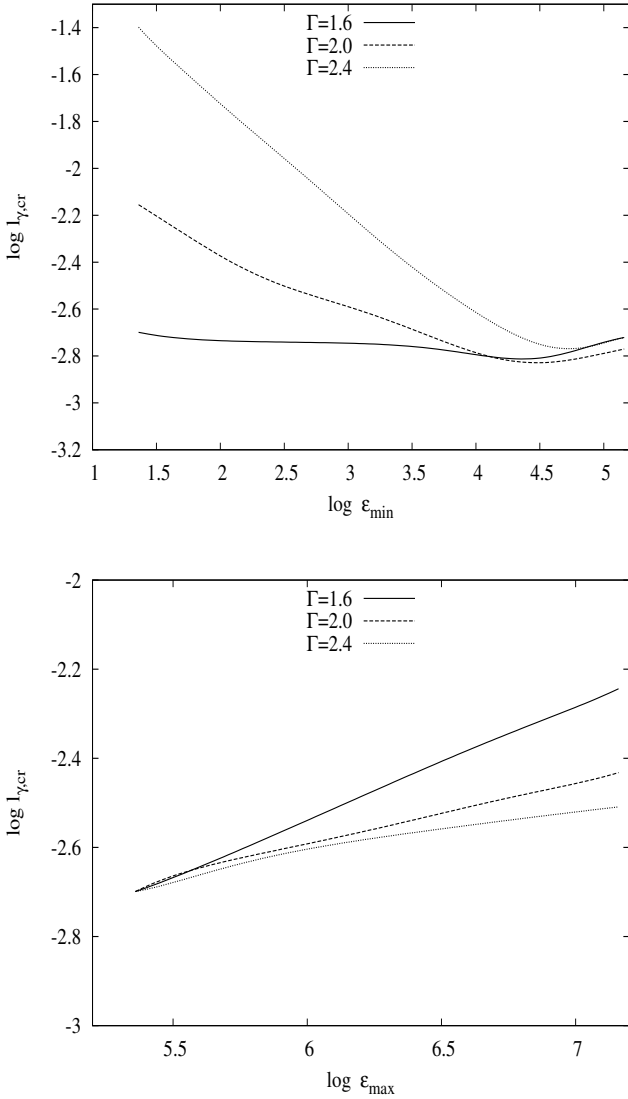


**Fig. 4.** Log-log diagram of the critical  $\gamma$ -ray compactness as a function of  $\epsilon_{\min}$  for constant  $\epsilon_{\max} = 2.3 \times 10^5$  (top panel) and as a function of  $\epsilon_{\max}$  for constant  $\epsilon_{\min} = 1.4 \times 10^5$  (bottom panel) for three photon indices marked on the plot. Other parameters used are:  $B = 40$  G and  $R = 3 \times 10^{16}$  cm.

### 3.2. Effects of a primary soft photon component

The main difference between automatic  $\gamma$ -ray absorption and the widely used photon-photon absorption on a pre-existing photon field (‘primary’ photons), is that in the first case no target field is initially present in the source. It is, as if the system finds its own equilibrium by self-producing the soft photons required for quenching the extra  $\gamma$ -ray luminosity. In many physical scenarios, however, primary photons are present in the source, e.g. synchrotron radiation from primary electrons, and therefore  $\gamma$ -rays are more likely to be absorbed on both primary and secondary photon fields. Here arises the question whether or not the effects of spontaneous photon quenching can be disentangled from those of linear absorption<sup>7</sup>.

<sup>7</sup> Some discussion on the subject in the context of differences in variability patterns can be found in PM12b.

In the limiting cases where  $\gamma$ -rays are being absorbed on either primary or secondary soft photons there is a straightforward relation between the photon index of the absorbed  $\gamma$ -ray spectrum and that of photon target field:

$$\Gamma_{abs} = \Gamma + s - 1, \text{ ‘linear’ quenching} \quad (45)$$

$$\Gamma_{abs} = \frac{3}{2}\Gamma, \text{ ‘non-linear’ quenching} \quad (46)$$

where  $s$  is the photon index of the primary photon distribution – see Appendix for the derivation of  $\Gamma_{abs}$  in the first case.

Using the numerical code presented in section 3 we will first verify the above analytical relations and then study intermediate cases. For this, we assume a spherical region with size  $R = 3 \times 10^{16}$  cm containing a magnetic field  $B = 40$  G. VHE  $\gamma$ -rays with a photon index  $\Gamma = 2.4$  are injected into this volume between energies  $\epsilon_{\min} = 23$  and  $\epsilon_{\max} = 2.3 \times 10^5$  with compactness  $\ell_{inj}$  being a free parameter. Primary photons are produced via synchrotron radiation of a power-law electron distribution with index  $p = 1.5$ . The maximum Lorentz factor  $\gamma_{\max}$  and the electron injection compactness  $\ell_{inj}^e$ , which is defined as  $\ell_{inj}^e = L_e^{inj} \sigma_T / 4\pi R m_e c^3$ , are also free parameters; here  $L_e^{inj}$  is the total electron injection luminosity. The only processes we consider in the following examples are synchrotron emission, photon-photon absorption and escape from the source. We note that the effect of inverse Compton scattering is negligible for the magnetic field and electron energies assumed here. The results regarding the two regimes are summarized in Fig. 5. In the top panel we have used  $\ell_{inj}^e = 10^{-7}$ ,  $\ell_{inj} = 8 \times 10^{-1} \gg \ell_{\gamma,cr}$  (solid line) and  $\ell_{inj}^e = 3 \times 10^{-2}$ ,  $\ell_{inj} = 8 \times 10^{-3} \ll \ell_{\gamma,cr}$  (dashed line), while we kept  $\gamma_{\max} = 3.6 \times 10^5$  fixed. For these parameter values the maximum energies of primary and secondary synchrotron photons are  $10^{-1}$  and  $1.3 \times 10^{-2}$  respectively. The slopes of different power-law segments in a  $x^2 n_\gamma(x)$  plot are also shown. The spectral break of the  $\gamma$ -ray spectrum differs between the two regimes and the numerical results are in agreement with those given by eqs. (45) and (46). In particular, we find that the absorbed  $\gamma$ -ray spectrum has a photon index  $\Gamma_{abs} = 3.5$  which should be compared to  $3\Gamma/2 = 3.6$  for the ‘non-linear’ quenching case. In order to estimate the spectral change for the ‘linear’ absorption case the photon index of the soft photon distribution is required, which in this example is  $s = (p/2) + 1 = 1.75$ . The expected value of  $\Gamma_{abs}$  is 3.15 while the derived one is 3. We note also that the spectral shape of the synchrotron component emitted by the produced pairs (solid line) is in agreement with that expected from our solution for the electron distribution – see eq. (38); emission from lower energy electrons ( $n_e \propto \gamma^{-2}$ ) results in  $n_\gamma \propto x^{-3/2}$ , while from higher energy electrons ( $n_e \propto \gamma^{-\Gamma-1}$ ) corresponds to  $n_s \propto x^{-\Gamma/2-1} = x^{-2.2}$ . In the bottom panel, along with the examples shown in the top panel (solid and dash-dotted lines), we plot two intermediate cases with a progressively higher  $\gamma$ -ray compactness, i.e.  $\ell_{inj} = 8 \times 10^{-2}$  (dashed line) and  $\ell_{inj} = 8 \times 10^{-1}$  (dotted line), while we used the same  $\ell_{inj}^e = 3 \times 10^{-2}$ . Already from  $\ell_{inj} = 8 \times 10^{-2}$ , which is still above the critical value, the contribution of photons produced via automatic  $\gamma$ -ray quenching is evident as a bump in the primary soft photon component. Notice also that the presence of primary soft photons enhances the auto-



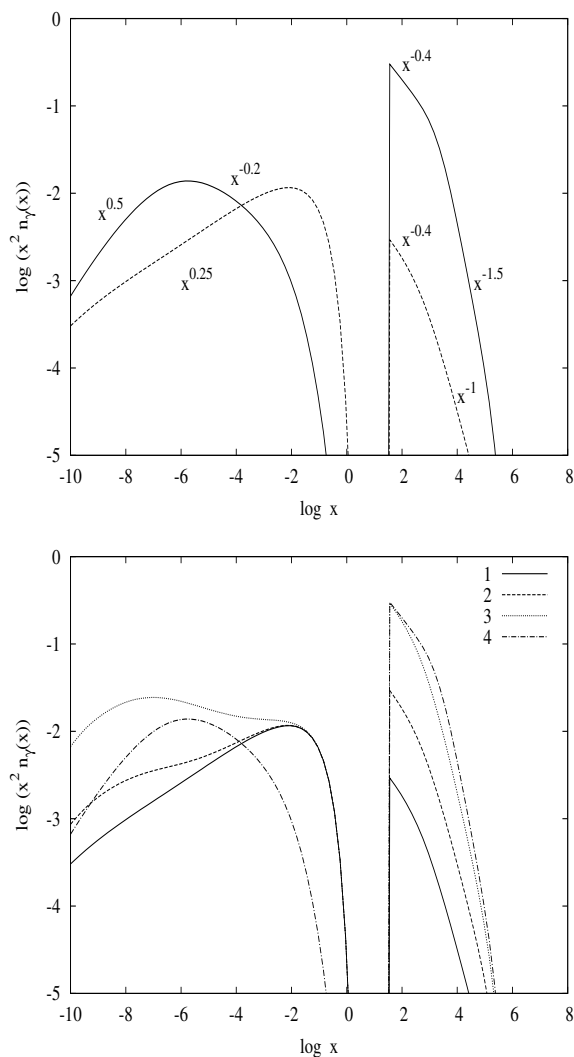


**Fig. 5.** Top panel: Comparison between two limiting cases where  $\gamma$ -ray photons are absorbed only on synchrotron photons emitted by secondary pairs (solid line) or by primary electrons (dashed line). The injection compactnesses of  $\gamma$ -rays and primary electrons are  $\ell_{\text{inj}} = 8 \times 10^{-1}$ ,  $\ell_{\text{inj}}^e = 10^{-7}$  (solid line) and  $\ell_{\text{inj}} = 8 \times 10^{-3}$ ,  $\ell_{\text{inj}}^e = 3 \times 10^{-2}$  (dashed line) respectively. Different parts of the spectra have different power-law dependencies that are marked on the plot. Bottom panel: Example of an intermediate case where  $\gamma$ -rays are being partially absorbed on synchrotron photons from secondaries. The injection compactness of primary electrons is  $\ell_{\text{inj}}^e = 3 \times 10^{-2}$ , while  $\ell_{\text{inj}}$  takes the following values:  $8 \times 10^{-3}$  (solid line),  $8 \times 10^{-2}$  (dashed line) and  $8 \times 10^{-1}$  (dotted line). The dash-dotted line that is obtained for  $\ell_{\text{inj}} = 8 \times 10^{-1}$ ,  $\ell_{\text{inj}}^e = 10^{-7}$  (same as solid line in top panel) is plotted for comparison reasons. Other parameters used for the plot are:  $B = 40$  G and  $R = 3 \times 10^{16}$  cm.

matic absorption of  $\gamma$ -rays for the same  $\ell_{\text{inj}}$  – compare the dotted and dash-dotted lines.

## 4. Implications on $\gamma$ -ray emitting blazars

### 4.1. General remarks

The mechanism of automatic photon quenching sets an upper limit to the intrinsic  $\gamma$ -ray luminosity of a compact source, and therefore, can be applied on  $\gamma$ -ray emit-

ting blazars for constraining physical quantities of their VHE emission region – for more details see PM11 and Petropoulou & Mastichiadis (2012a) – hereafter PM12a. This can be relevant to recent observations that have revealed the presence of very hard intrinsic TeV  $\gamma$ -ray spectra of blazars, even when corrected with low EBL flux levels, e.g. 1ES 1101-232 (Aharonian et al. 2006), 1ES 0229+200 (Aharonian et al. 2007). The SEDs of some hard  $\gamma$ -ray sources are very difficult to be explained within one-zone emission models, and therefore, they are often attributed to a second component, whose emission in longer wavelengths is hidden by that of the first component (e.g. Costamante (2012)). Thus, the physical conditions of the component emitting in the TeV energy range can be chosen quite arbitrarily only by demanding to fit the VHE part of the spectrum. The presence of very hard TeV  $\gamma$ -ray spectra (typically  $\Gamma_{\text{int}} \simeq 1.5$ ) implies that these sources cannot be spontaneously quenched, i.e. their intrinsic  $\gamma$ -ray luminosity should be less than the critical one. We note, however, that there is an alternative scenario that employs the photon-photon absorption on internal soft photon fields exactly for explaining the formation of very hard intrinsic  $\gamma$ -ray spectra (Aharonian et al. 2008).

By now there are several (quasi)simultaneous observations of blazars in the GeV and TeV energy range, which clearly show that the  $\gamma$ -ray spectrum cannot be fitted by a simple power-law over the whole GeV-TeV energy range, but rather by a broken power-law. The change of the photon index in many cases is large ( $\Delta\Gamma \gtrsim 1$ ) and it cannot be explained using simple arguments, such as cooling breaks ( $\Delta\Gamma = 0.5$ ). In particular, for high-peaked blazars that are bright in the *Fermi* energy band (e.g. Mrk421, PKS 2155-304, PKS 0447-439 etc.), the peak of their SED seems to fall in the high-GeV energy part of the spectrum ( $\simeq 100$  GeV). In these cases GeV and TeV emission correspond to parts of the spectrum below and above the high-energy hump respectively. Thus, it is commonly considered that the VHE  $\gamma$ -ray spectra are intrinsically much softer (e.g. exponential cutoff effects) than the GeV-spectra (Costamante 2012).

Here, however, we investigate another explanation of  $\gamma$ -ray spectral breaks. In our framework, the *injection*  $\gamma$ -ray spectrum is described by a single power-law from GeV up to TeV energies, and the spectrum of the *escaping*  $\gamma$ -ray radiation is modified due to internal spontaneous photon absorption. We remind that the instability of automatic photon quenching offers an alternative mechanism for producing intrinsic broken power-law spectra (see section 2).

A plot of the photon index in the GeV energy band (as measured by the *Fermi* satellite) versus the one in the TeV energy band (as measured by MAGIC and H.E.S.S. telescopes) is shown in Fig. 6. The sources used for this plot are listed in Table 1 along with the observed values of the photon indices and the reference paper. Filled and open symbols show the photon indices of the observed and of the corrected for EBL absorption VHE spectra. We note that in all cases we used the model C by Finke et al. (2010) for the EBL correction; in this model, the EBL flux from UV to the near-IR is also similar to that of Domínguez et al. (2011). Different symbols, in particular circles and squares, denote TeV observations made by MAGIC and H.E.S.S. respectively. The solid line represents the relation between the photon indices that is expected by spontaneous photon quenching, i.e.  $\Gamma_{\text{TeV}} = 3\Gamma_{\text{GeV}}/2$ , whereas the dashed line ( $\Gamma_{\text{TeV}} = \Gamma_{\text{GeV}}$ ) is plotted only for guiding the eye.

**Table 1.** Photon indices of the GeV- and TeV- $\gamma$ -ray spectrum for the sources used in Fig. 6. Their redshift and the reference papers are also listed.

	Source	$\Gamma_{\text{TeV}}$	$\Gamma_{\text{GeV}}^1$	$z$	Reference
MAGIC	1ES 1215+303	$2.96 \pm 0.14$	$2.0 \pm 0.2$	0.130	Aleksić et al. (2012a)
	NGC 1275	$4.1 \pm 0.7$	$2.17 \pm 0.05$	0.018	Aleksić et al. (2012b)
	Mrk 421	$2.48 \pm 0.03$	$1.75 \pm 0.03$	0.031	Abdo et al. (2011b)
	PKS 1222+21	$3.75 \pm 0.27$	$1.95 \pm 0.21$	0.43	Aleksić et al. (2011a)
	3C 279	$3.1 \pm 1.1$	$2.3 \pm 0.1$	0.536	Abdo et al. (2009b); Aleksić et al. (2011b)
	IC 310	$2.00 \pm 0.14$	$1.58 \pm 0.25$	0.019	Aleksić et al. (2010)
	Mrk 501	$2.51 \pm 0.05$	$1.78 \pm 0.03^2$	0.034	Abdo et al. (2011a)
H.E.S.S.	1ES 0414+009	$3.45 \pm 0.25$	$1.85 \pm 0.18$	0.287	H.E.S.S. Collaboration et al. (2012)
	PKS 2005-489	$3.20 \pm 0.16$	$1.79 \pm 0.07$	0.071	H.E.S.S. Collaboration et al. (2011)
	PKS 0447-439	<b><math>3.89 \pm 0.37</math></b>	<b><math>1.85 \pm 0.035</math></b>	0.2 <sup>3</sup>	H.E.S.S. Collaboration et al. (2013)
VERITAS	RGB J0710+591	$2.69 \pm 0.26$	$1.46 \pm 0.17$	0.125	Acciari et al. (2010b)
	PKS 1424+240	$3.8 \pm 0.5$	$1.8 \pm 0.07$	unknown	Acciari et al. (2010a)
	RJX 0648.7+516	$4.4 \pm 0.8$	$1.89 \pm 0.1$	0.179	Aliu et al. (2011)
	RBS 0413	$3.18 \pm 0.68$	$1.57 \pm 0.12$	0.19	Aliu et al. (2012)

<sup>1</sup> All observations in the GeV energy band are made with *Fermi* satellite. For the specific energy range where the photon index is calculated see corresponding reference.

<sup>2</sup> Photon index of the average GeV spectrum.

<sup>3</sup> Although the redshift of this source is still disputed, we use the value 0.2 that is in agreement with most of the present estimates in literature.

Some of the data points within their error bars are compatible with the theoretical predictions. For the purposes of the present work, the choice of a particular EBL model does not affect significantly our results. For example, the EBL model used here predicts slightly higher optical depth than the one of Franceschini et al. (2008) for  $E_\gamma \lesssim 5$  TeV (10 TeV) for  $z = 0.6$  (0.1), respectively. Thus, correction of the VHE spectra with the EBL model of Franceschini et al. (2008) would result in slightly softer intrinsic VHE spectra, i.e. some of the open symbols in Fig. 6 would move upwards in the vertical direction. Moreover, the fact that the analysis of the *Fermi* and MAGIC/H.E.S.S./VERITAS data has not been made over the same energy intervals for all sources listed in Table 1 makes difficult the derivation of any conclusions regarding the statistical properties of this sample. Non-simultaneity of GeV and TeV observations in some cases, e.g. NGC 1275, makes also any coherent comparison difficult. For these reasons, this type of plot could be used only as a *first indicator* for searching among sources that could be explained by the mechanism of automatic quenching.

In these cases, there are five additional features that can be tested observationally:

- (i) Automatic photon quenching is a radiative instability that redistributes the energy within a photon population. The absorbed  $\gamma$ -ray luminosity appears, therefore, in the lower part of the multiwavelength (MW) spectrum—usually in the X-ray regime.
- (ii) The spectral break in the  $\gamma$ -ray spectrum of blazars that have low X-ray emission with respect to that of VHE  $\gamma$ -rays can, in general, not be attributed to automatic photon absorption.
- (iii) If the VHE  $\gamma$ -ray spectrum is spontaneously absorbed, there is a straightforward relation between the photon

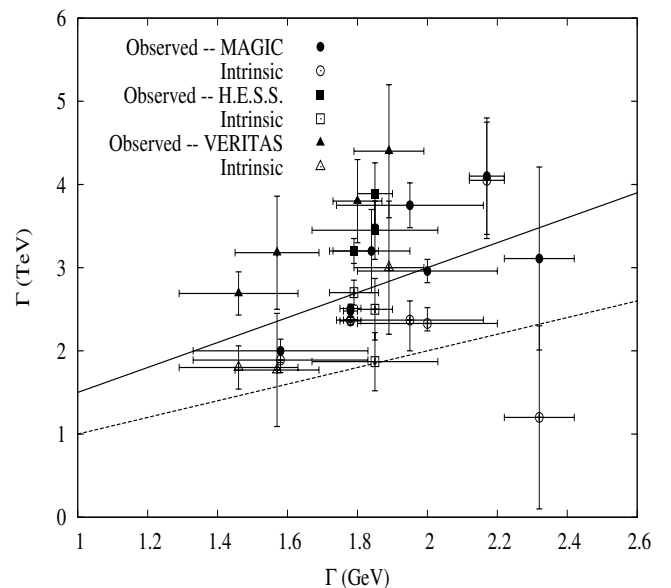


**Fig. 6.** Photon index of the TeV spectrum versus the one of the GeV spectrum for several  $\gamma$ -ray emitting blazars.

indices of the absorbed part of the  $\gamma$ -ray spectrum and that of the soft photon component. In Section 2.3 we have shown that  $\Gamma_{\text{abs}} = 3\Gamma/2$ , where  $\Gamma$  is the photon index of the  $\gamma$ -ray spectrum at injection. The steady state electron distribution due to pair production is  $n_e(\gamma) \propto \gamma^{-\Gamma-1}$  – see eq. (38) – and the corresponding photon index of the synchrotron spectrum is given by  $\Gamma_{\text{soft}} = \Gamma/2 + 1$ . Thus, the relation between the two

photon indices is  $\Gamma_{\text{abs}} = 3(\Gamma_{\text{soft}} - 1)$  – see also the numerical example in the top panel of Fig. 5.

- (iv) Strong correlation between the soft component of the MW spectrum and the unabsorbed part of the  $\gamma$ -ray spectrum is to be expected in case where the intrinsic  $\gamma$ -ray luminosity varies.
- (v) An increase of the intrinsic  $\gamma$ -ray compactness is accompanied by a shift of the break energy towards lower energies.

As far as the first observational prediction is concerned, one can show that the maximum energy of the soft component produced by automatic photon quenching, falls, for reasonable parameter values, in the X-ray regime. First, the ‘feedback’ criterion for automatic quenching must be satisfied, at least, by  $\gamma$ -ray photons having the maximum energy (see also section 2). This is written as

$$B > B_q \equiv (4 \times 10^{-5}) \delta^3 (1+z)^{-3} (E_{\text{max},12}^{\text{obs}})^{-3} \text{ in G,} \quad (47)$$

where we have used the observed quantities instead of those measured in the comoving frame of the blob that has a Doppler factor  $\delta$ . From this point on and in what follows the convention  $E_X \equiv E/10^X$  in eV will be adopted for photon energies, unless stated otherwise<sup>8</sup>. In section 2 we have shown that a spontaneously quenched  $\gamma$ -ray spectrum shows a break at the energy  $\epsilon_{\text{br}} = 8B_{\text{cr}}/(B\epsilon_{\text{max}}^2)$ . Combining this expression with the fact that the observed break energy  $E_{\text{br}}^{\text{obs}}$  usually lies in the GeV energy band, we derive a second relation between the magnetic field and the Doppler factor of the blob

$$B_{\text{br}} = (4 \times 10^{-2}) \delta^3 (1+z)^{-3} (E_{\text{max},12}^{\text{obs}})^{-2} (E_{\text{br},9}^{\text{obs}})^{-1} \text{ in G,} \quad (48)$$

Since the break energy is by definition smaller than the maximum one, the magnetic field  $B_{\text{br}}$  always satisfies inequality (47). We note that the magnetic field required is, generally, strong. Even for a small value of the Doppler factor, e.g.  $\delta = 10$ , one needs  $B \simeq 40$  G – see also PM12a for a related discussion. Thus, spontaneously quenched  $\gamma$ -ray spectra cannot operate in the context of one-zone leptonic models, such as synchrotron-self Compton (SSC) that usually requires weak magnetic fields (e.g. Böttcher et al. (2009)). Finally, the observed maximum energy of the produced soft photons is given by

$$E_{s,\text{max}}^{\text{obs}} = 0.5 \delta^2 (1+z)^{-2} (E_{\text{br},9}^{\text{obs}})^{-1} \text{ in keV} \quad (49)$$

where we have used the magnetic field strength given by eq. (48).

If a  $\gamma$ -ray emitting blazar happens to be a spontaneously quenched source, then one can make a strong prediction about the flux correlation between soft (usually X-ray) photons, the unabsorbed part of the  $\gamma$ -ray spectrum (GeV energy band) and the absorbed one (typically TeV energy band). Increase of the intrinsic  $\gamma$ -ray compactness amplifies, in general, the absorption of VHE  $\gamma$ -rays, which leads to an increase of the soft photon component. The number of photon targets for the  $\gamma$ -rays is then increased, which further sustains the non-linear loop of photon-photon absorption. The part of the  $\gamma$ -ray spectrum that is not

<sup>8</sup> Capital and small initial letters are used for differentiating between photon energies with and without dimensions respectively.

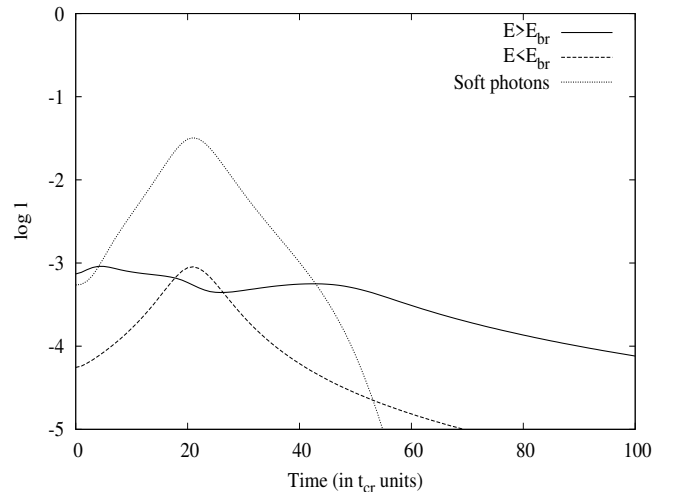


**Fig. 7.** Plot of photon compactness as a function of time for various components: absorbed and unabsorbed  $\gamma$ -rays are plotted with solid and dashed lines respectively, while soft photons are shown with a dotted line. Parameters used for this plot:  $\epsilon_{\text{max}} = 2.3 \times 10^5$ ,  $\epsilon_{\text{min}} = 23$ ,  $\Gamma = 1.5$ ,  $B = 40$  G,  $R = 3 \times 10^{16}$  cm,  $\ell_{\text{inj}} = 1.7 \times 10^{-3} \gtrsim \ell_{\gamma,\text{cr}}$ ,  $G = 10$  and  $\tau_c = 20$ .

affected by automatic quenching follows exactly the variations of the injection compactness, whereas the spontaneously quenched varies in the inverse way. The above are exemplified in Fig. 7. First, we allowed the system to reach a steady state – for the parameters used see caption of Fig. 7. Then, we imposed on the injected  $\gamma$ -ray compactness a Lorentzian variation

$$\ell_{\text{inj}}(\tau) = (\ell_{\text{inj}})_0 \frac{F_L(\tau)}{F_L(0)} \quad (50)$$

where  $\tau$  is the comoving time in units of  $t_{\text{cr}}$  and

$$F_L(\tau) = \frac{\frac{G}{2\pi}}{(\tau - \tau_c)^2 + \left(\frac{G}{2\pi}\right)^2} \quad (51)$$

where  $\tau_c, G$  are free parameters that control the position of the maximum and the width at half maximum respectively. Then, we calculated the photon compactness of the soft component ( $x \leq b\epsilon_{\text{max}}^2/4$ ), of the unabsorbed ( $\epsilon_{\text{min}} \leq \epsilon \leq 10\epsilon_{\text{min}} \approx \epsilon_{\text{br}}$ ) and spontaneously quenched ( $0.1\epsilon_{\text{max}} \leq \epsilon \leq \epsilon_{\text{max}}$ )  $\gamma$ -rays and plotted them as a function of time in Fig. 7. The evolution of the break energy of the spectrum from high to lower energies can be seen in Fig. 8, where snapshots of MW spectra are plotted.

#### 4.2. Application to blazar PKS 0447-439

PKS 0447-439 is a bright blazar that has been recently detected at high energy (Abdo et al. 2009a) and VHE (H.E.S.S. Collaboration et al. 2013)  $\gamma$ -rays. Although the redshift of the source is still disputable (see e.g. Prandini et al. (2012); Pita et al. (2012) for different estimations and discussion), in the following we will adopt the value  $z = 0.2$ . Furthermore, a higher redshift, that is equivalent to a larger optical depth for  $\gamma\gamma$  absorption, would imply a harder intrinsic VHE spectrum and therefore a smaller value of  $\Delta\Gamma \equiv \Gamma_{\text{TeV}} - \Gamma_{\text{GeV}}$ . However, taking into account the errorbars of the photon indices, a fit can still

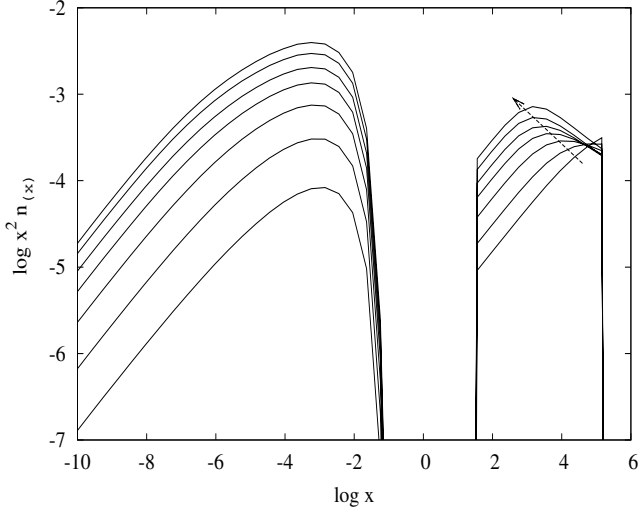


**Fig. 8.** Snapshots of MW spectra obtained for a variable  $\gamma$ -ray injection compactness. The type of variation and the parameter values are the same as in Fig. 7. The arrow shows the ‘hard-to-soft’ evolution of the  $\gamma$ -ray spectrum break energy.

be achieved for a range of redshift values ( $0.1 < z < 0.24$ ). We have focused on PKS 0447-439 since it satisfies most of the conditions that were presented in the previous section. In particular:

- The photon indices in the GeV- and TeV- energy range are  $\Gamma_{\text{GeV}} = 1.85 \pm 0.05$  and  $\Gamma_{\text{TeV}} \approx 2.5 \pm 0.37$  respectively<sup>9</sup>. This is in agreement with what we have shown, i.e. a  $\gamma$ -ray spectrum with  $\Gamma = 1.8$  can steepen up to  $\Gamma = 2.7$  due to spontaneous quenching.
- The X-ray luminosity is less than the  $\gamma$ -ray one but of the same order of magnitude.
- An anticorrelated variability between VHE  $\gamma$ -rays and X-rays may be suggested, although the number of data points is small and therefore still inconclusive – see Fig. 5 in H.E.S.S. Collaboration et al. (2013).

As a first attempt, we did not specify the production mechanism of  $\gamma$ -rays. Instead, we have assumed that they are being injected into the emission region with a rate given by

$$Q_\gamma = Q_0 \epsilon^{-\Gamma} H(\epsilon - \epsilon_{\min}) H(\epsilon_{\max} - \epsilon), \quad (52)$$

where  $Q_0$  is a normalization constant that is related to the injection  $\gamma$ -ray compactness as

$$Q_0 = \begin{cases} 3\ell_{\text{inj}} \ln\left(\frac{\epsilon_{\max}}{\epsilon_{\min}}\right)^{-1}, & \text{if } \Gamma = 2 \\ 3\ell_{\text{inj}}(\Gamma - 2) (\epsilon_{\min}^{-\Gamma+2} - \epsilon_{\max}^{-\Gamma+2})^{-1}, & \text{if } \Gamma \neq 2. \end{cases} \quad (53)$$

We have also included the injection of primary electrons at a rate

$$Q_{\text{inj}}^e = Q_{0,e} \gamma^{-p} H(\gamma - \gamma_{\min}) H(\gamma_{\max} - \gamma), \quad (54)$$

where  $Q_{0,e}$  is related to the electron injection compactness in the same way as in eq. (53). The parameters of the fit shown in Fig. 9 can be found in Table 2.

<sup>9</sup> The VHE photon index is calculated after correcting for EBL absorption for  $z = 0.2$  and using the model by Finke et al. (2010).

**Table 2.** Parameters for multiwavelength fit to the observations of PKS 0447-439 during the period November 2009-January 2010 (see Fig. 9).

Parameter symbol	
$R$ (cm)	$8 \times 10^{15}$
$B$ (G)	20
$u_B$ (erg cm <sup>-3</sup> )	16
$\delta$	11
$\epsilon_{\max}$ ( $m_e c^2$ )	$10^5$
$\epsilon_{\min}$ ( $m_e c^2$ )	$10^{-6}$
$\Gamma$	1.8
$\ell_{\text{inj}}$	$7.2 \times 10^{-3}$
$\ell_{\gamma, \text{cr}}$	$2 \times 10^{-3}$
$\gamma_{\max}$	$8 \times 10^3$
$\gamma_{\min}$	$8 \times 10^2$
$p$	2.5
$\ell_{\text{inj}}^e$	$2 \times 10^{-3}$

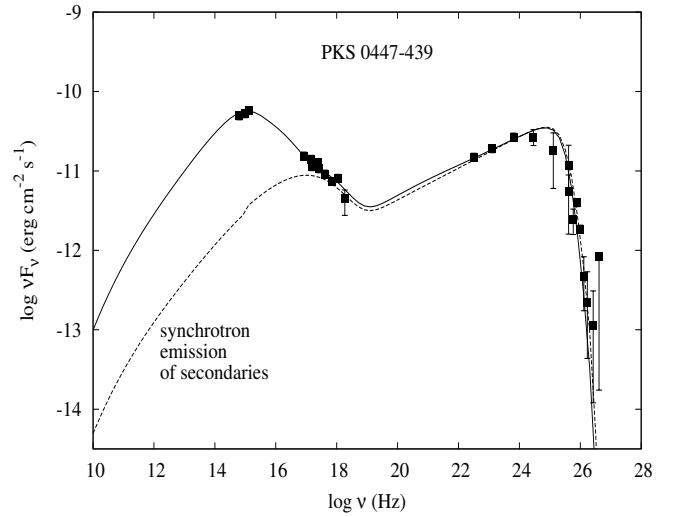


**Fig. 9.** Multiwavelength spectrum of PKS 0447-439 during the period November 2009-January 2010. Filled squares represent the *Swift*/UVOT, *Swift*/XRT, *Fermi* and H.E.S.S. data from low to high energies respectively. Solid and dashed lines show the SEDs with and without the injection of primary electrons. Our model SEDs are corrected for EBL absorption assuming  $z = 0.2$  and using model C of Finke et al. (2010).

Figure 9 shows that the synchrotron emission of secondary electron/positron pairs explains the X-ray emission, while the synchrotron emission from primary leptons is required for fitting the optical data. In this example, primary soft photons, i.e. photons that are not produced by automatic quenching of  $\gamma$ -rays, are not targets for photon-photon absorption due to their low energies, and therefore, ‘linear’ absorption does not interfere with the non-linear one. We note that inverse Compton scattering was taken also into account; both primary and secondary soft photon fields were used in the scatterings. As a second step, one could attribute  $\gamma$ -ray emission to a particular production mechanism, e.g. to synchrotron radiation from relativistic protons, since the choice of a relatively large value of the magnetic field makes the application of automatic photon quenching more relevant to hadronic emission models;

a detailed hadronic modelling of the source lies, however, outside from the scope of the present paper.

## 5. Discussion

A very interesting, yet largely unnoticed, property of  $\gamma$ -ray radiation transfer is the presence of an upper limit at the production rate per volume of  $\gamma$ -ray photons. If the  $\gamma$ -ray compactness at injection exceeds this critical value, then soft photons are produced spontaneously in the source, serve as targets for high-energy photons and absorb the ‘excessive’  $\gamma$ -ray luminosity. Thus, soft photons act as a thermostat and appear irrespective of the  $\gamma$ -ray production mechanism. These ideas were put forward in SK07, who coined the term ‘automatic photon quenching’ to describe this non-linear mechanism, and were expanded by PM11 and PM12b. The present paper continues the exploration of automatic quenching in the case where  $\gamma$ -rays are injected with a power-law distribution. Therefore, this can be considered as a continuation of an earlier work (PM11), in which the quenching in the case of monoenergetic  $\gamma$ -ray injection was studied.

In section 2 we have derived an analytical expression of the critical compactness that is required for an injected power-law  $\gamma$ -ray spectrum to be quenched. A series of approximations/assumptions, which were presented in detail in the same section, were necessary for the above derivation. In particular, the ‘catastrophic losses’ approximation for electrons proved to be crude enough and made our analytical results valid in a particular parameter range; we have commented on that through an indicative example, where the analytically and numerically derived values of the critical compactness were compared. In cases where automatic photon quenching applies, we have calculated the steady-state  $\gamma$ -ray spectra and shown that spontaneous photon absorption produces a break of  $\Delta\Gamma = \Gamma/2$  between the unabsorbed and the absorbed parts of the injected power-law; here  $\Gamma$  is the slope of the injected  $\gamma$ -rays.

In section 3 we have implemented a numerical code that solves the full radiative transfer problem inside a spherical volume, in order to derive the critical  $\gamma$ -ray compactness for a wide range of parameter values, e.g. for various photon indices, as well as for different minimum and maximum energies of the  $\gamma$ -ray spectrum. We have also examined the effects that a primary soft photon component would have on the absorption of  $\gamma$ -rays. We found that these depend on both the compactness and the spectral shape of the external component.

In §4 we have examined the implications of quenching on  $\gamma$ -ray emitting blazars. We have also given a set of criteria that can be used in order to deduce, observationally, whether a  $\gamma$ -ray blazar is spontaneously quenched or not. We note that the relevant information is imprinted both on the SED and on the variability patterns of the source. We also point out that blazar PKS 0477-439 meets several of the criteria and there is a distinct possibility that its high-energy spectrum is quenched, while the X-rays are produced from the reprocessing of  $\gamma$ -rays.

In the present paper we have intentionally avoided pinpointing a specific mechanism for  $\gamma$ -ray production. However, the range of parameters used and especially the choice of a rather large magnetic field value (of the order of a few Gauss), imply that these ideas are more effectively applied to hadronic models. In this case  $\gamma$ -rays could be produced

either by proton-synchrotron radiation or by pion production (Mastichiadis et al. 2013).

Automatic quenching might have some far-reaching implications for  $\gamma$ -ray blazars. If there is evidence that it operates at some level, then part (or all) of the UV/X-ray component should be reprocessed  $\gamma$ -ray emission, i.e. there is no need for a primary component to produce all of the observed soft radiation. It also predicts that, for AGN related parameters, breaks in the  $\gamma$ -ray spectra should appear in the high GeV – low TeV regime. Moreover, a ‘hard-to-soft’ evolution of the spectral break is expected whenever the injected  $\gamma$ -ray flux increases. Therefore, future observations, especially with CTA (Sol et al. 2013), could prove decisive in detecting the presence of such spectral breaks. If, on the other hand, the sources do not show signs of spontaneous quenching, then some interesting constraints apply to the source parameters, as this relates the  $\gamma$ -ray luminosity to the size of the source, the magnetic field strength and the Doppler factor – see PM12a for such an application on quasar 3C 279. These constraints can be quite severe, especially if the source undergoes strong flaring episodes and the absence of quenching could only mean either a very large value of the Doppler factor or a low magnetic field in the production region. Both aspects have strong implications for the physical conditions prevailing in the emitting regions of  $\gamma$ -ray blazars.

*Acknowledgements.* We would like to thank the anonymous referee for useful comments/suggestions on the manuscript and Dimitri Ligri for helping us compile Table 1. This research has been co-financed by the European Union (European Social Fund – ESF) and Greek national funds through the Operational Program "Education and Lifelong Learning" of the National Strategic Reference Framework (NSRF) - Research Funding Program: Heracleitus II. Investing in knowledge society through the European Social Fund.

## Appendix A: $\gamma$ -ray spectral break due to absorption on primary soft photons

We derive the spectral break of a  $\gamma$ -ray spectrum due to the absorption of a primary soft photon component ( $n_{\text{ex}}$ ) that is present in the emission region. In this case, the absorption of  $\gamma$ -rays is a ‘linear’ process in contrast to automatic quenching. We treat the target photon population as a photon ‘tank’, in the sense that  $n_{\text{ex}}$  does not evolve with time. Thus, the steady-state  $\gamma$ -ray photon spectrum is derived by solving the same set of equations as those presented in section 2.3, with the operator  $\mathcal{L}_{\gamma\gamma}^{\gamma}$  (and  $Q_{\gamma\gamma}^e$ ) being slightly different:

$$\mathcal{L}_{\gamma\gamma}^{\gamma} = -\frac{n_{\gamma}(\epsilon)\sigma_0}{\epsilon} \int_{2/\epsilon}^{X_M} dx x^{-1} (n_s(x) + n_{\text{ex}}(x)) \quad (\text{A.1})$$

where  $X_M = \max[x_{\text{max}}, x_0]$  and  $x_{\text{max}}, x_0$  are the maximum energies of the secondary and primary soft photons respectively. The above expression represents the most general physical case, where  $\gamma$ -rays are being absorbed by both primary and secondary soft photons. One can distinguish between two regimes:

1. spontaneously or ‘non-linear’  $\gamma$ -ray absorption, if  $n_{\text{ex}}(x) \ll n_s(x)$
2. ‘linear’  $\gamma$ -ray absorption, if  $n_{\text{ex}}(x) \gg n_s(x)$ .

Here we focus on the second regime, where after following the same steps as those described in section 2.3, we find the steady-state  $\gamma$ -ray distribution

$$n_{\gamma}(\epsilon) \approx \frac{Q_{\gamma}(\epsilon)}{1 + \frac{\sigma_0 n_0}{\epsilon} \int_{2/\epsilon}^{x_0} dx x^{-s-1}}, \quad (\text{A.2})$$

where  $n_0$  is the normalization of the primary soft photon distribution. Since we are interested in calculating the photon index of the absorbed part of the spectrum it is sufficient to look at the asymptotic expression of  $n_{\gamma}(\epsilon)$ ,

$$n_{\gamma}(\epsilon) \rightarrow \epsilon^{-\Gamma-s+1} \quad (\text{A.3})$$

which is obtained for  $\epsilon^{s-1} \gg 2^s s / \sigma_0 n_0$ . Thus, in this regime the spectral break is given by

$$\Delta\Gamma = s - 1. \quad (\text{A.4})$$

## References

- Abdo, A. A., Ackermann, M., Ajello, M., et al. 2011a, *ApJ*, 727, 129  
 Abdo, A. A., Ackermann, M., Ajello, M., et al. 2009a, *ApJS*, 183, 46  
 Abdo, A. A., Ackermann, M., Ajello, M., et al. 2009b, *ApJ*, 700, 597  
 Abdo, A. A., Ackermann, M., Ajello, M., et al. 2011b, *ApJ*, 736, 131  
 Acciari, V. A., Aliu, E., Arlen, T., et al. 2010a, *ApJ*, 708, L100  
 Acciari, V. A., Aliu, E., Arlen, T., et al. 2010b, *ApJ*, 715, L49  
 Aharonian, F., Akhperjanian, A. G., Barres de Almeida, U., et al. 2007, *A&A*, 475, L9  
 Aharonian, F., Akhperjanian, A. G., Bazer-Bachi, A. R., et al. 2006, *Nature*, 440, 1018  
 Aharonian, F. A., Khangulyan, D., & Costamante, L. 2008, *MNRAS*, 387, 1206  
 Aleksić, J., Alvarez, E. A., Antonelli, L. A., et al. 2012a, *A&A*, 544, A142  
 Aleksić, J., Alvarez, E. A., Antonelli, L. A., et al. 2012b, *A&A*, 539, L2  
 Aleksić, J., Antonelli, L. A., Antoranz, P., et al. 2010, *ApJ*, 723, L207  
 Aleksić, J., Antonelli, L. A., Antoranz, P., et al. 2011a, *ApJ*, 730, L8  
 Aleksić, J., Antonelli, L. A., Antoranz, P., et al. 2011b, *A&A*, 530, A4  
 Aliu, E., Archambault, S., Arlen, T., et al. 2012, *ApJ*, 750, 94  
 Aliu, E., Aune, T., Beilicke, M., et al. 2011, *ApJ*, 742, 127  
 Böttcher, M. & Chiang, J. 2002, *ApJ*, 581, 127  
 Böttcher, M., Reimer, A., & Marscher, A. P. 2009, *ApJ*, 703, 1168  
 Coppi, P. S. 1992, *MNRAS*, 258, 657  
 Coppi, P. S. & Blandford, R. D. 1990, *MNRAS*, 245, 453  
 Costamante, L. 2012, *ArXiv e-prints*, 1208.0810  
 Domínguez, A., Primack, J. R., Rosario, D. J., et al. 2011, *MNRAS*, 410, 2556  
 Finke, J. D., Razzaque, S., & Dermer, C. D. 2010, *ApJ*, 712, 238  
 Franceschini, A., Rodighiero, G., & Vaccari, M. 2008, *A&A*, 487, 837  
 Herterich, K. 1974, *Nature*, 250, 311  
 H.E.S.S. Collaboration, Abramowski, A., Acero, F., et al. 2012, *A&A*, 538, A103  
 H.E.S.S. Collaboration, Abramowski, A., Acero, F., et al. 2011, *A&A*, 533, A110  
 H.E.S.S. Collaboration, Abramowski, A., Acero, F., et al. 2013, *A&A*, 552, A118  
 Jelley, J. V. 1966, *Nature*, 211, 472  
 Kataoka, J., Takahashi, T., Makino, F., et al. 2000, *ApJ*, 528, 243  
 Katarzyński, K., Ghisellini, G., Tavecchio, F., et al. 2005, *A&A*, 433, 479  
 Kazanas, D. 1984, *ApJ*, 287, 112  
 Kirk, J. G. & Mastichiadis, A. 1992, *Nature*, 360, 135  
 Konopelko, A., Mastichiadis, A., Kirk, J., de Jager, O. C., & Stecker, F. W. 2003, *ApJ*, 597, 851  
 Mastichiadis, A. & Kirk, J. G. 1995, *A&A*, 295, 613  
 Mastichiadis, A. & Kirk, J. G. 1997, *A&A*, 320, 19  
 Mastichiadis, A., Petropoulou, M., & Dimitrakoudis, S. 2013, *ArXiv e-prints*  
 Mastichiadis, A., Protheroe, R. J., & Kirk, J. G. 2005, *A&A*, 433, 765  
 Petropoulou, M. & Mastichiadis, A. 2009, *A&A*, 507, 599  
 Petropoulou, M. & Mastichiadis, A. 2011, *A&A*, 532, A11  
 Petropoulou, M. & Mastichiadis, A. 2012a, *MNRAS*, 426, 462  
 Petropoulou, M. & Mastichiadis, A. 2012b, *MNRAS*, 421, 2325  
 Pita, S., Goldoni, P., Boisson, C., et al. 2012, in *American Institute of Physics Conference Series*, Vol. 1505, American Institute of Physics Conference Series, ed. F. A. Aharonian, W. Hofmann, & F. M. Rieger, 566–569  
 Prandini, E., Bonmoli, G., & Tavecchio, F. 2012, *A&A*, 543, A111  
 Protheroe, R. J. 1986, *MNRAS*, 221, 769  
 Sol, H., Zech, A., Boisson, C., et al. 2013, *Astroparticle Physics*, 43, 215  
 Stawarz, L. & Kirk, J. G. 2007, *ApJ*, 661, L17  
 Stern, B. E., Begelman, M. C., Sikora, M., & Svensson, R. 1995, *MNRAS*, 272, 291  
 Svensson, R. 1987, *MNRAS*, 227, 403  
 Zdziarski, A. A. & Lightman, A. P. 1985, *ApJ*, 294, L79